Adsorption (2007) 13: 425–437
DOI 10.1007/s10450-007-9034-4

Argon and krypton adsorption on templated mesoporous silicas: molecular simulation and experiment

Francisco R. Hung · Supriyo Bhattacharya · Benoit Coasne · Matthias Thommes · Keith E. Gubbins

Received: 29 April 2007 / Revised: 17 July 2007 / Accepted: 23 July 2007 / Published online: 21 September 2007
© Springer Science+Business Media, LLC 2007

Abstract In this work we report molecular simulation results for argon and krypton adsorption on atomistic models of templated mesoporous silica materials. These models add atomistic levels of detail to mesoscale representations of these porous materials, which were originally generated from lattice Monte Carlo simulations mimicking the synthesis process of templated mesoporous silicas. We generate our atomistic pore models by carving out of a silica block a 'mathematically-smooth' representation of the pores from lattice MC simulations. Following that procedure, we obtain a model material with mean mesopore and micropore diameters of 5.4 nm and 1.1 nm, respectively (model A). Two additional model materials were considered: one with no microporosity, and with mesopores similar to those of model A (model B), and a regular cylindrical pore (model C). Simulation results for Ar and Kr adsorption on these model materials at 77 K and 87 K shows that model A provides the best agreement with experimental data; however, our results suggest that fine-tuning the microporosity and/or the surface chemistry (i.e., by decreasing the density of OH groups at the pore surface) of model A can lead to better agreement with experiments. The filling of the mesopores in model materials A and B proceeded via a classical capillary condensation mechanism, where the pores fill at slightly different pressures. This observation contrasts with what was observed in our previous study (Coasne, et al. in Langmuir 22:194–202, 2006), where we considered atomistic silica mesopores with an important degree of surface roughness at length scales below 10 Å, for which we observed a quasi-continuous mesopore filling involving intermediate phases with liquid-like "bridges" and gas-like regions. These results suggest that pore surface roughness, and other morphological features such as constrictions, play an important role in the mechanism of adsorption and filling of the mesopores.

Keywords Templated mesoporous silica materials · MCM-41 · SBA-15 · Gas adsorption · Molecular simulation · Monte Carlo

F.R. Hung
Department of Chemical and Biological Engineering, University of Wisconsin, Madison, WI 53706-1691, USA

S. Bhattacharya · K.E. Gubbins (✉)
Center for High Performance Simulation and Department of Chemical and Biomolecular Engineering, North Carolina State University, Raleigh, NC 27695-7905, USA
e-mail: keg@ncsu.edu

S. Bhattacharya
City of Hope National Medical Center, Beckman Research Institute, Duarte, CA 91010, USA

B. Coasne
Institut Charles Gerhardt Montpellier, CNRS (UMR 56253), University Montpellier 2, and ENSCM, 34095 Montpellier cedex 5, France

M. Thommes
Quantachrome Instruments, Boynton Beach, FL 33426, USA

Present address:
F.R. Hung
Cain Department of Chemical Engineering Louisiana State University, Baton Rouge, LA 70803, USA

1 Introduction

Templated mesoporous silica materials MCM-41 and SBA-15 (Kresge et al. 1992; Zhao et al. 1998a, 1998b) are obtained by a template mechanism involving the formation of surfactant or block copolymers micelles, in a mixture

composed of a solvent and a silica source. After polymerization of the silica and removal of the organic micelles, one obtains a material made up of a hexagonal array of cylindrical pores. As a result, MCM-41 and SBA-15 consist of hexagonal arrays of cylindrical pores with diameters between 1.5 and 20 nm, and narrow pore size distributions. These properties make these materials ideal for fundamental studies aimed at determining the effect of surface forces, confinement and reduced dimensionality on the phase behavior of guest molecules. The features of these silica materials also make them suitable for a number of applications in catalysis, adsorption, optics, as low dielectric constant materials to insulate integrated circuits, and as host materials for polymers, nanoparticles and enzymes (Ciesla and Schüth 1999; Selvam et al. 2001; Soler-Illia et al. 2002; Schüth and Schmidt 2002). However, and despite extensive studies using Transmission Electronic Microscopy (TEM), X-ray diffraction and adsorption experiments (Ciesla and Schüth 1999; Selvam et al. 2001; Soler-Illia et al. 2002; Schüth and Schmidt 2002), there are some uncertainties in some aspects of the surface chemistry and texture of these materials (impurities, defects, microporosity, surface roughness, etc.) (Edler et al. 1998; Sonwane et al. 1999; Berenguer-Murcia et al. 2002). For instance, it has been shown that the cylindrical mesopores in SBA-15 materials are connected through transverse microporous channels (Imperor-Clerc et al. 2000; Ryoo et al. 2000; Galarneau et al. 2001). On the other hand, it is generally agreed that MCM-41 is made up of unconnected mesopores (Ryoo et al. 2000; Jun et al. 2000). The gas-liquid transition of adsorbates in templated mesoporous silica materials has been extensively studied by experiment, theory and molecular simulation (Gelb et al. 1999). A number of silica pore models with regular geometry have been used recently in molecular simulation studies (Maddox et al. 1997; Koh et al. 1999; Gelb 2002; He and Seaton 2003; Kuchta et al. 2004; Coasne and Pellenq 2004a, 2004b; Puibasset 2005a) to consider adsorption of different pure substances and mixtures on MCM-41 type materials. However, it is unclear whether these regular models are realistic representations of templated mesoporous silicas, since some experimental studies (Edler et al. 1998; Sonwane et al. 1999) suggest that these materials exhibit a smooth surface at molecular scales (3–7 Å) with roughness and other morphological defects (constrictions and tortuosity) at larger length scales (20–50 Å).

One possible approach to model porous solids is to mimic the synthesis process of the real material using simulations, a strategy used in the past (Gelb and Gubbins 1998, 1999a) to develop realistic models for Vycor and controlled pore glasses (CPG). The formation of ordered porous structures in templated mesoporous materials is directly related to the phenomenon of self-assembly of surfactants or block copolymers. The timescales involved in the formation of micelles involving these species are in the range of microseconds to milliseconds. Therefore, modeling such a process with appropriate system sizes and an atomistic representation of all the chemical species is highly difficult, even with state-of-the-art computing facilities. As a result, mesoscale lattice Monte Carlo simulations with a coarse-grained representation of the surfactant chains and the different solvent species were used recently to study the behavior of surfactant-inorganic oxide-solvent systems, and mimic the synthesis of templated mesoporous silica materials (Siperstein and Gubbins 2001, 2003; Bhattacharya and Gubbins 2005). Low values of the surfactant/inorganic oxide concentration ratio led to formation of hexagonally ordered porous structures that resemble that of templated mesoporous silicas. Atomistic levels of detail were added to these mesoscale models in recent studies (Coasne et al. 2005, 2006b; Hung et al. 2006), by carving out of a silica block the skeleton of the MCM-41 mesoscale pore model obtained by Siperstein and Gubbins (Siperstein and Gubbins 2001, 2003). Simulations of gas adsorption on this model material, and comparisons with experimental results, showed that this silica mesopore model exhibited pore walls with excessive pore surface roughness as compared to real materials, at length scales below 10 Å. Nevertheless, its simulated small angle neutron scattering (SANS) spectrum shows that its pore roughness at larger length scales (10–50 Å) were in agreement with experimental results for MCM-41 (Edler et al. 1998; Sonwane et al. 1999).

Other atomistic models have been developed recently for templated mesoporous silicas. Sonwane and coworkers (Sonwane et al. 2005) introduced silicon and oxygen atoms around cylindrical templates, and they introduced surface roughness by creating spherical voids at random locations inside the pore walls, until the skeletal silica density was equal to the experimental value of 2.2 g/cm^3. Schumacher et al. (Schumacher et al. 2006a) modeled the synthesis process of templated mesoporous silicas with a kinetic Monte Carlo method and simplified potentials, using predefined geometries for the templating micelles. They further extended their methodology to develop models of periodic mesoporous silicas with their surfaces doped with organic functional groups (Schumacher et al. 2006b). In the models of Sonwane et al. and Schumacher et al., the templating micelles have a predefined, simple shape (spherical or cylindrical). In experiments, however, the diameter of a cylindrical micelle can fluctuate along the cylinder axis, which can create undulations on the pore surface of the resulting templated mesoporous silica. Given that our earlier atomistic models of templated mesoporous silica (Coasne et al. 2005, 2006a; Hung et al. 2006) exhibited pore undulations at length scales between 10–50 Å which were in agreement with experimental results, in this work we attempt to improve our atomistic pore models by reducing its surface roughness at length

scales below 10 Å. To do that, we use b-splines (Piegl and Tiller 1997) to obtain a 'mathematically-smooth' representation of the pore surfaces from the mesoscale, lattice MC simulations, and then carve out this pore morphology from a silica block. We have also developed a scheme for incorporating the micropores in the atomistic model, by carving the surfactant chains out of the silica walls. To the best of our knowledge, this is one of the first attempts at incorporating micropores in a molecular model of SBA-15. We have simulated Ar and Kr adsorption on this atomistic silica model (model A, which included mesopores and micropores). Ar adsorption is a key standard measurement for characterization of porous materials (Gregg and Sing 1982; Llewellyn et al. 1996, 1997; Rouquerol et al. 1999). Due to its low vapor pressure, Kr adsorption at low temperatures (77 K, 87 K) is starting to be used (Llewellyn et al. 1996, 1997; Takei and Chikazawa 1998; Chiu et al. 2006; Zukal 2006; Thommes et al. 2007) in the characterization of materials with very low surface areas, such as the thin films of mesoporous silica used as low dielectric constant materials in microelectronics (Schüth and Schmidt 2002). We also simulate the gas adsorption on two additional model materials: one with no microporosity, but with mesopores similar to those of model A (model B), and a model material with a single regular cylindrical mesopore (model C). We compare our simulated adsorption isotherms and isosteric heat of adsorption with available experimental results, and we discuss the adsorption and pore filling mechanisms in our model materials. The rest of the paper is organized as follows. In Sect. 2 we present details of the preparation of our model silica materials, and details of our simulations for gas adsorptions. Our results are presented and discussed in Sect. 3. Section 4 includes some concluding remarks and suggestions for future work.

2 Models and methods

2.1 Preparation of the model silica mesoporous materials

The mimetic simulation procedure to obtain mesoscale, lattice models of templated mesoporous silica materials has been described in detail in previous publications (Siperstein and Gubbins 2001, 2003; Bhattacharya and Gubbins 2005). Atomistic levels of detail are then incorporated into the mesoscale model of Bhattacharya and Gubbins (Bhattacharya and Gubbins 2005; see Fig. 1), by following a methodology similar to that presented in our previous publications (Coasne et al. 2005, 2006a; Hung et al. 2006). However, our early silica models exhibited pore walls with excessive surface roughness at length scales below 10 Å, as compared with real materials. In order to reduce such surface roughness in our silica pore models, we have incorporated the suggestions prescribed in our previous publications (Coasne et al. 2006a; Hung et al. 2006). To generate an atomistic model of templated mesoporous silica, based on the pore morphologies obtained from the lattice MC simulations, we use a methodology that is as follows. First, the lattice positions of the inorganic oxide segments from the mimetic simulations are scaled assuming a lattice unit of 0.5 nm, to obtain a material with an average mesopore diameter of $D_{meso} = 5.4$ nm and a pore length of $L = 15$ nm. The choice of such a lattice spacing is motivated by the fact that it corresponds to a reasonable approximation for the size of the bead in the lattice simulations (a few SiO_2 tetrahedron units per bead). Moreover, similar values of lattice spacings were also used in previous lattice Monte Carlo studies of self-assembly of surfactants performed by our group (Lísal et al. 2002; Siperstein and Gubbins 2003; Scanu et al. 2004; Bhattacharya and Gubbins 2005). Then, we isolate one of the pores from the lattice MC simulations, and identify silica particles that are on the pore surface. We then use b-splines (Piegl and Tiller 1997) to obtain a smooth mathematical representation of the pore surface; the control points of the b-splines are given by the coordinates of the silica particles (Fig. 1). We then carve out this pore surface from the center of an atomistic box with $19 \times 12 \times 21$ unit cells of non-porous cristoballite (a siliceous non-porous solid), corresponding to a simulation box of 13.5 nm $\times$8.5 nm $\times$14.9 nm. The procedure is repeated for a second pore from the lattice MC simulations; however, for this case the pore was divided in four sections, which are then carved out from the four corners of the simulation box (Fig. 1). This is equivalent to having two mesopores in our simulation box, due to the use of periodic boundary conditions in our computer simulations. To illustrate this point, we have included in Fig. 1 the structure that is obtained by replicating our simulation box twice in the x and y directions. This structure exhibits a hexagonal array of cylindrical pores, average distance between mesopores of $\sim$9 nm and silica walls thicknesses of $\sim$4 nm, in agreement to what was reported for SBA-15 materials (average distance between mesopores of $\sim$11 nm, silica wall thicknesses of 3.1–6.4 nm) (Zhao et al. 1998b).

The next step in our procedure is to carve out the micropores from the atomistic silica box (Fig. 1). The position of the micropores is given by the coordinates of the surfactant chains, which are obtained from the lattice MC simulations. Experimental evidence (Galarneau et al. 2003) indicates that micropores in SBA-15 materials have a diameter ranging from 0.5 to 1.5 nm. Therefore, in our model the micropore diameters are randomly selected from a Gaussian distribution with a mean value of 1.1 nm. After including the microporosity in our model, we remove the silicon atoms that are in an incomplete tetrahedral environment, as well

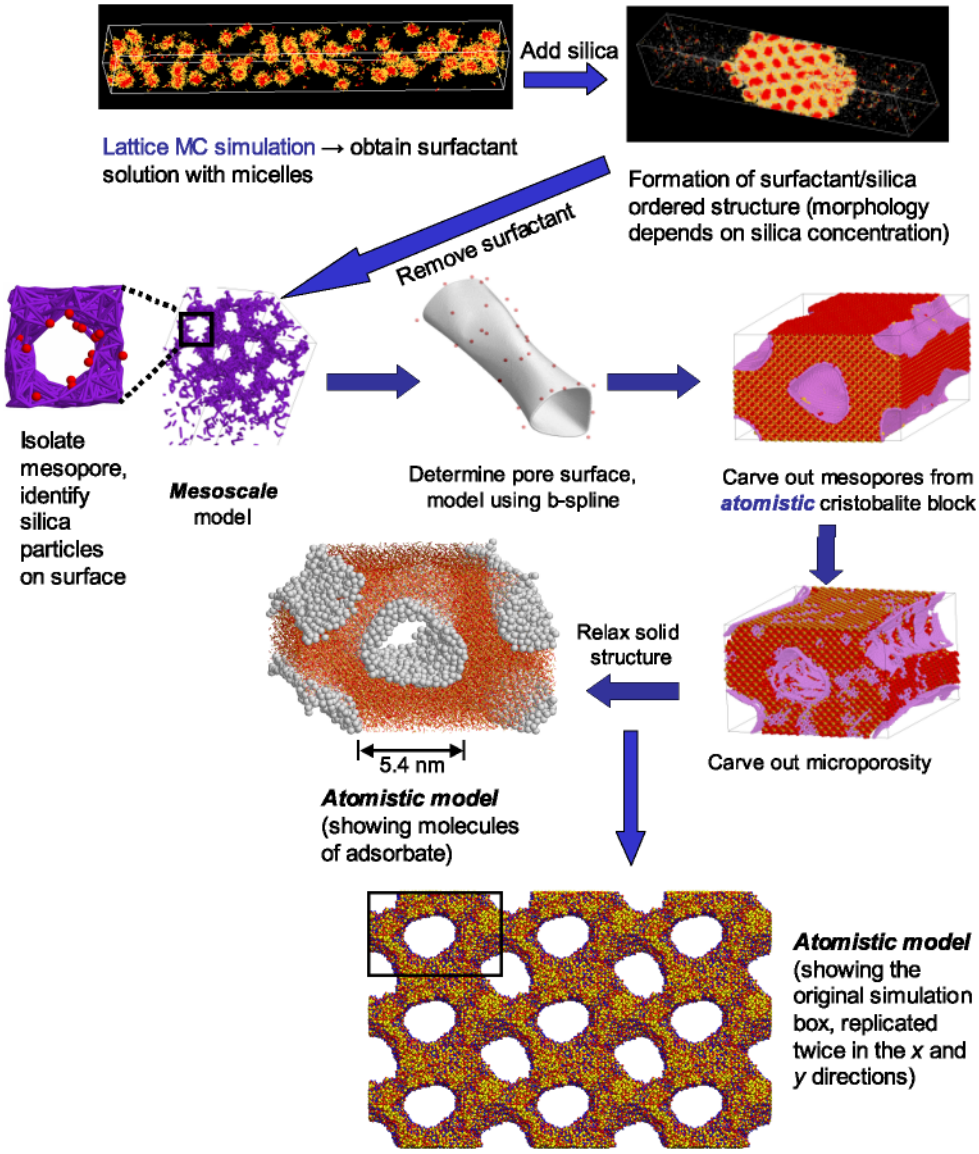

Fig. 1 (Color online) Scheme of the procedure used to generate the atomistic silica pore model A, from a mesoscale model of templated mesoporous silica (Bhattacharya and Gubbins 2005)

as the oxygen atoms with two dangling bonds. This procedure ensures that no silicon atoms have dangling bonds, all oxygen atoms have at least one saturated bond with a silicon atom, and the pore surface is modeled in a realistic way. To ensure that the atomistic simulation box has no net electrical charge, oxygen atoms with one dangling bond are saturated with hydrogen atoms; these are placed perpendicularly to the pore surface (in the pore voids), at a distance of 1 Å from the closest unsaturated oxygen atom. It has been shown (Pellenq and Levitz 2002) that the density of OH groups obtained using such a procedure is close to that obtained experimentally for porous silica glasses (7–8 OH per nm^2) (Landmesser et al. 1997). On the other hand, the density of OH groups reported experimentally at the surface of templated mesoporous silicas is usually smaller, 2–3 OH per nm^2 (for a detailed discussion, see Coasne et al. 2006b). Despite this quantitative difference in the surface chemistry of the model material and the experimental samples, it has been shown that the simulated materials obtained using the procedure described above are able to capture adsorption and condensation of fluids in nanoporous silicas (Coasne and Pellenq 2004a, 2004b; Coasne et al. 2005, 2006a, 2006b; Hung et al. 2006). Moreover, the discussion on the effect of the existence of morphological defects by comparing the simulations for regular and constricted silica pores is relevant since the surface chemistry is the same for all samples. To mimic the amorphous silica surface exhibited by experimental samples of templated mesoporous silicas, we sightly displace all the O, Si and H atoms a random distance, following previous studies (Pellenq and Levitz 2002). The final structure is shown in Fig. 1; such a structure corresponds to a basic unit for the structure of hexagonally ordered SBA-15. Our methodology to generate atomistic silica pores is based on techniques originally proposed by Pellenq and Levitz (Pel-

lenq and Levitz 2002) to model Vycor glasses. Coasne and Pellenq (Coasne and Pellenq 2004a, 2004b; Coasne et al. 2006b) extended these techniques to prepare silica pores of various morphologies and/or topologies, such as cylindrical, hexagonal, ellipsoidal and constricted pores.

In Fig. 2 we compare the pore size distribution (PSD) of our model material to that of an experimental sample of a SBA-15 material (Ryoo et al. 2000). In the experiments of Ryoo et al., the pore size distributions were calculated using the Barret, Joyner and Halenda (BJH) algorithm (Rouquerol et al. 1999); the relation between the pore size and the capillary condensation pressure was calibrated in a previous study using MCM-41 silicas (Kruk et al. 1997). The PSD in our model material was determined by following a procedure outlined in previous reports (Gelb and Gubbins 1999b; Bhattacharya and Gubbins 2006). We select points randomly and uniformly distributed in the simulation box, and determine the 'geometrical pore size' at each of the points. The geometrical pore size at a given point is defined as the largest sphere that can be constructed, that encompasses the given point and does not overlap any atom of the neighboring walls (Gelb and Gubbins 1999b; Bhattacharya and Gubbins 2006). Then we construct a cumulative histogram $H(D)$ representing the probability of finding a point in the model space with a pore diameter greater than or equal to D. The pore size distribution $P(D)$ is then defined as:

$$P(D) = -\frac{dH(D)}{dD}. \quad (1)$$

Gelb and Gubbins (Gelb and Gubbins 1999b) and Coasne et al. (Coasne et al. 2004) have applied the BJH method to different model porous materials, and compared the BJH PSDs against the 'exact' PSDs. They considered model material with pores of different morphologies and topologies (Vycor-like materials, cylindrical and ellipsoidal pores, and cylindrical pores with constrictions). Both studies concluded that the BJH method gives PSDs that are shifted to lower pore sizes (by roughly 1–2 nm) when compared to the 'exact' PSD of the model materials. Nevertheless, the BJH method is able to provide PSDs that are closer to the 'exact' PSD for model materials with pore sizes larger than 5 nm. The reason behind this behavior is that the BJH method is based on the Kelvin equation, which breaks down for pore sizes smaller than 10 nm (Gelb et al. 1999; Thommes 2004; and references therein).

From Fig. 2, we can say that the model and the experimental PSDs are qualitatively similar with bimodal distributions, where the rightmost peak represents the mesoporosity and the leftmost peak the microporosity. The mean mesopore and micropore diameters in our model are 5.4 nm and 1.1 nm, respectively. For the experimental sample, the mean diameters are 6 nm and 1.06 nm for the mesopores and micropores. The width of the mesopore peak is 2 nm in both the model and the experimental samples. The microporous volume in our model (assuming the micropores have pore sizes below 2 nm) represents 28% of the total porosity. Our model material has a higher micropore volume compared to the experimental material of Ryoo and coworkers; however, for other samples of SBA-15 the microporosity can represent 30% of the total porosity (Galarneau et al. 2001). Our model also shows some secondary porosity between 2 and 4 nm, which is a characteristic of experimental SBA-15 materials that are heated to high temperatures after synthesis (Galarneau et al. 2001). The experimental material from Ryoo et al. also shows some secondary porosity, although the amount is less than that of the model. The total pore volume in our model is 0.77 cm^3/g, which is in agreement with the values obtained from the experiments (Ryoo et al. 2000; Galarneau et al. 2001). More details and characterization properties of our model materials will be provided in a forthcoming publication (Bhattacharya et al. 2007).

We used a similar simulation protocol to generate two additional model materials. No microporosity is present in model B, and the mesopores are similar to those in model A. Model C consists of a regular cylindrical mesopore with no microporosity. Front views and transverse cross sections of the three models are depicted in Fig. 3. The mean mesopore diameter in all three models is $D = 5.4$ nm; nevertheless, by comparing the cross section views of pore models A and B (Fig. 3), it is apparent that the elimination of microporosity leads to a small reduction in the mesopore diameter of model B. Model A represents a SBA-15 material, and model B represents a non-microporous silica material such as MCM-41; however, the silica walls in model B are about 2–4 times thicker than those observed in real MCM-41 materials (∼4.1 nm in model B, ∼1–1.5 nm in MCM-41 materials). Model C will be used to analyze how the adsorption properties of models A and B differ from those in an ideal, cylindrical pore model.

2.2 Gas adsorption

Argon and krypton are modeled as Lennard-Jones (LJ) fluids with the following parameters (Pellenq and Levitz 2002): $\sigma_{Ar} = 0.34$ nm, $\varepsilon_{Ar}/k_B T = 120$ K, $\sigma_{Kr} = 0.369$ nm, $\varepsilon_{Kr}/k_B T = 170$ K. The interaction of Ar and Kr atoms with O, Si and H atoms in the substrate is modeled using the PN-TraZ potentials and parameters, which have been used successfully in the past to model gas adsorption in zeolites (Pellenq and Nicholson 1994) and Vycor glass (Pellenq and Levitz 2002). In this potential, the interaction energy U_i of a rare gas atom i with the substrate is given by:

$$U_i = \sum_{j\in\{O,Si,H\}} \left[A_{ij} e^{-b_{ij} r_{ij}} - \sum_{n=3}^{5} f_{2n} \frac{C_{2n,ij}}{r_{ij}^{2n}} \right] - \frac{\alpha_i E_i^2}{2}, \quad (2)$$

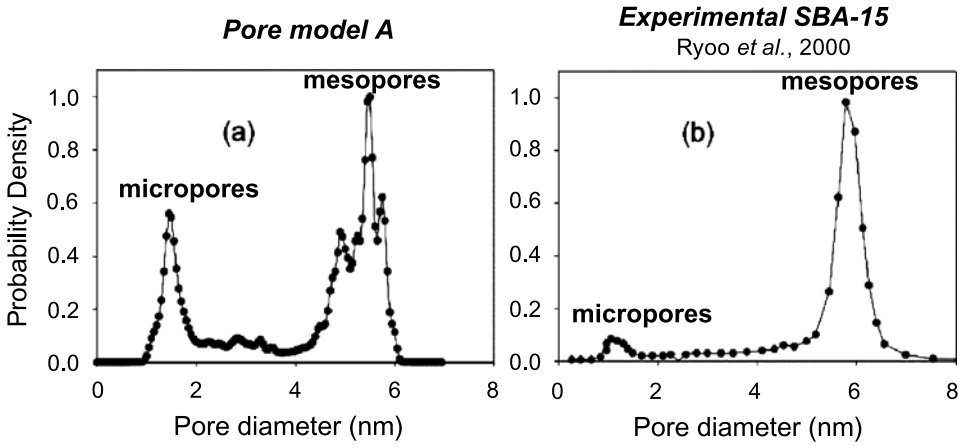

Fig. 2 Pore size distributions; (**a**) model material (model A), (**b**) experimental SBA-15 (Ryoo et al. 2000)

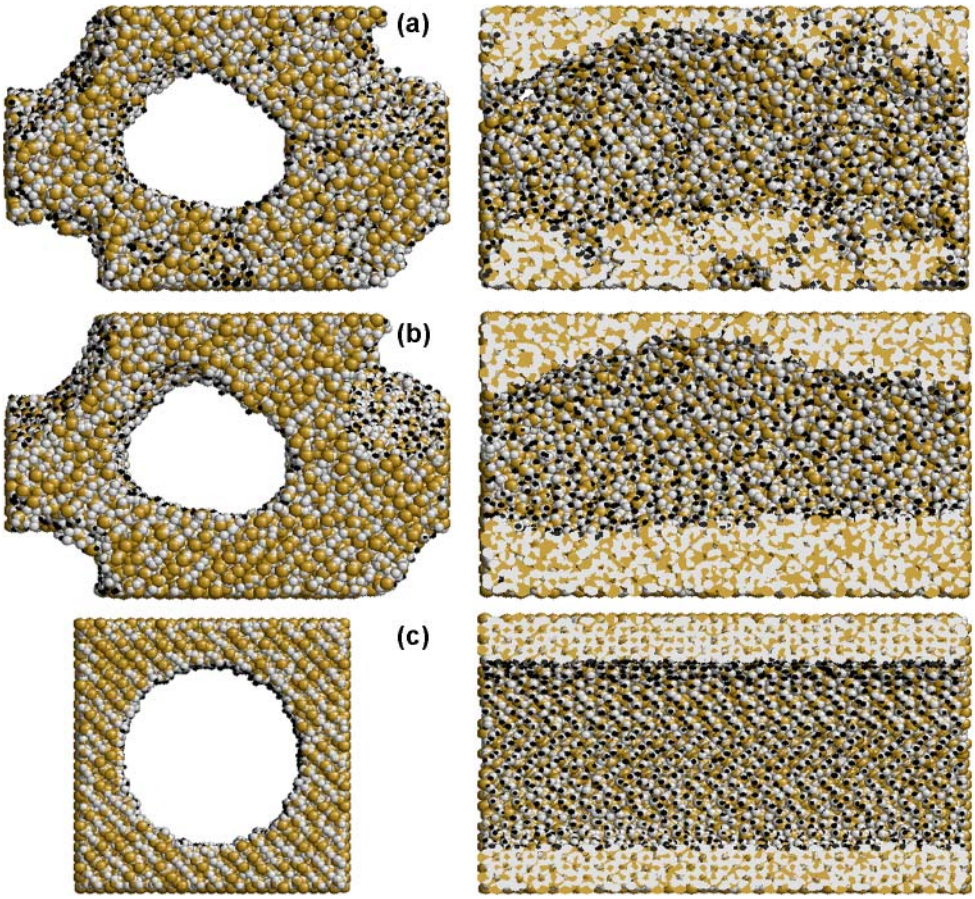

Fig. 3 (Color online) Front views and cross section views of the different models used in this study. Silicon, oxygen and hydrogen are represented in *tan*, *grey* and *black*. Model A was generated through the procedure schematized in Fig. 1, and exhibits both mesoporosity and microporosity. Model B has mesopores that are similar to those of model A, but has its microporosity removed. Model C is a regular cylindrical pore model. All three models have a mean mesopore diameter of 5.4 nm

$$f_{2n} = 1 - \sum_{k=0}^{2n} \frac{(b_{ij} r_{ij})^k}{k!} \exp(-b_{ij} r_{ij}) \tag{3}$$

where the sum runs over all atoms in the substrate (Si, O and H). The terms in (2) represent the short-range repulsion, the dispersion interaction and the induction interaction, respectively (Pellenq and Levitz 2002). The f_{2n} terms represent damping functions which vary steeply from 0 up to 1 as the distance r_{ij} between the two atoms involved increases. Values of the gas-substrate interaction parameters, as well as more details of the intermolecular potential functions, can be found in previous publications (Pellenq and Levitz 2002).

We performed Grand Canonical Monte Carlo (GCMC) (Nicholson and Parsonage 1982; Allen and Tildesley 1987; Frenkel and Smit 2002) simulations of Ar and Kr adsorption at $T = 77$ K and 87 K, respectively. The ideal gas equation and the properties of the LJ fluid at coexistence (Kofke 1993; Johnson et al. 1993; Agrawal and Kofke 1995) were used to calculate chemical potentials μ from relative pressures

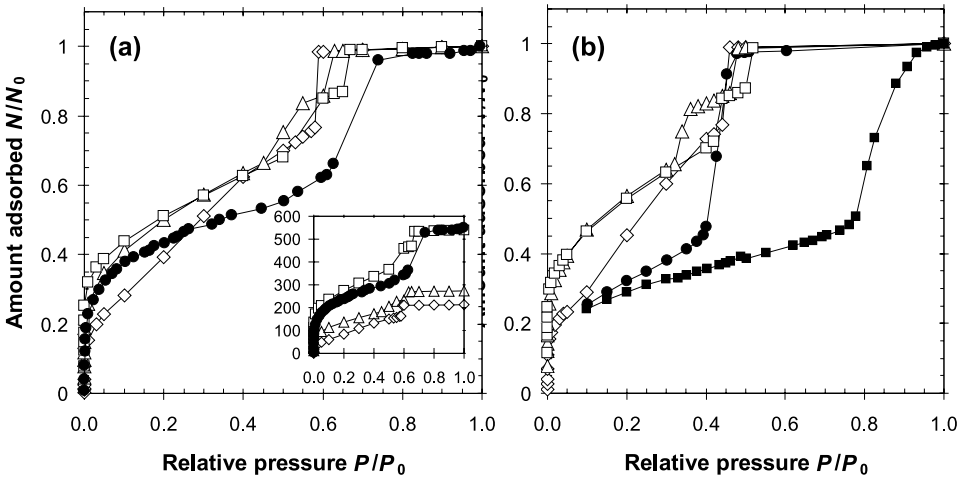

Fig. 4 Adsorption isotherms for (**a**) Ar at $T = 77$ K, and (**b**) Kr at $T = 87$ K. Simulation results for pore models A, B and C are depicted by *open squares*, *triangles* and *diamonds*, respectively. Experimental results for Ar adsorption at 77 K on SBA-15 with a mean mesopore diameter of $D = 5$ nm (Galarneau et al. 2003) are represented in Fig. 4(a) by *black circles*. Experimental results for Kr adsorption at 87 K on MCM-41 and SBA-15 with mean mesopore sizes of $D = 4.2$ nm and $D = 6.3$ nm (Thommes et al. 2007) are depicted in Fig. 4(b) by *black circles* and *squares*, respectively. The *inset* in Fig. 4(a) represents adsorption data, in cm^3 of Ar at standard T and P per gram of adsorbent, as a function of relative pressure P/P_0

P/P_0. To speed up our simulation runs, we have used an energy grid (Pellenq and Levitz 2002; Coasne et al. 2006a) with an elementary cube size of about 1 $Å^3$ to compute the adsorbate-wall potential energy. An accurate estimation of the energy is then obtained by linearly interpolating between the grid values. Thermodynamic properties were averaged over a minimum of 10^5 MC steps per particle (typical systems had up to $N = 20\,000$ particles); however, much longer runs were considered near the phase transitions. We also determined the isosteric heat of adsorption, q_{st} (Nicholson and Parsonage 1982):

$$q_{st} = q_{st}^{ff} + q_{st}^{fw} = \left[RT - \frac{\langle U_{ff}N\rangle - \langle U_{ff}\rangle\langle N\rangle}{\langle N^2\rangle - \langle N\rangle^2}\right] + \left[-\frac{\langle U_{fw}N\rangle - \langle U_{fw}\rangle\langle N\rangle}{\langle N^2\rangle - \langle N\rangle^2}\right] \quad (4)$$

where q_{st}^{ff}, q_{st}^{fw} represent the adsorbate-adsorbate and the adsorbate-wall contributions to q_{st}. The quantities in brackets $\langle\cdots\rangle$ represent ensemble averages, R is the gas constant, and U_{ff} and U_{fw} represent the adsorbate-adsorbate and adsorbate-wall potential energy. Periodic boundary conditions were applied in the three directions x, y and z. Such conditions allow a realistic representation of the adsorption behavior.

We did not study the desorption behavior in our systems. Realistic modeling of such phenomena requires the presence of an interface between the fluid in the pores and in the bulk, and thus larger systems need to be considered (Gelb 2002; Coasne et al. 2006b). Likewise, we have not studied hysteresis in our systems. The physics behind hysteresis in confined fluids is still not clearly understood, especially for disordered porous matrices, and currently is an active area of research (see, e.g. Evans 1990; Gelb et al. 1999; Rouquerol et al. 1999; Sarkisov and Monson 2001; Gelb 2002; Vishnyakov and Neimark 2003; Coasne and Pellenq 2004a, 2004b; Thommes 2004). In a previous work (Coasne et al. 2006a) we found that surface disorder in the pore reduces the width of the hysteresis loop. This result is due to the fact that surface roughness makes it easier to nucleate the liquid phase, and thus it helps to overcome metastability barriers upon adsorption. It was also found that the hysteresis loops for such pores with an important degree of surface roughness is rather asymmetric (the desorption branch is steeper than the adsorption branch), when compared to the hysteresis loops obtained for smooth cylindrical pores.

3 Results and discussion

3.1 Adsorption isotherms and isosteric heat of adsorption

The adsorption isotherms of argon (at 77 K) and krypton (at 87 K) on the three atomistic silica mesopore models are presented in Fig. 4. The adsorbed amounts have been normalized to the total number of atoms, N_0, when the pores are filled. At a fixed T, the adsorption curves as a function of relative pressure P/P_0 exhibit different features and are significantly affected by the pore morphology. For the regular cylindrical pore model (model C), we observe one small vertical jump in the adsorption curves, which is due to capillary

condensation inside the pore. In contrast, two small jumps are observed in the adsorption isotherms for pore models A (with micropores) and B (without micropores). On the one hand, the surface area of pore model A is larger than that of model B due to the presence of microporosity and surface roughness, where the molecules of adsorbate can be preferentially adsorbed at lower values of P/P_0. On the other hand, pore undulations and other morphological features on the mesopores cause the surface area of model B to be larger than that of model C. As a result, at low pressures ($P/P_0 < 0.4$ for Ar, $P/P_0 < 0.3$ for Kr), pore model A exhibits the largest amount adsorbed, followed by models B and C. A small increase in P/P_0 leads to the first small jump in the adsorption isotherm of model B. This is due to the fact that elimination of microporosity in model B leads to a small reduction in its mesopore diameter, as compared to the other pore models (see the cross section views in Fig. 3). Further increases in P/P_0 leads, in order, to the following features in the adsorption isotherms: first jump (model A), second jump (model B), single jump (model C), and second jump (model A). The three pore models fill at similar values of P/P_0, around 0.60–0.65 for Ar (Fig. 4(a)) and around 0.5 for Kr (Fig. 4(b)). As will be discussed in the following section, the two jumps for model A and model B correspond to capillary condensation in each mesopore (the simulation box for both models contains two mesopores).

In Fig. 4 we compare our simulation results with experimental data for gas adsorption on several templated mesoporous silica samples (Galarneau et al. 2003; Thommes et al. 2007). We consider first the case of Kr adsorption at 87 K (Fig. 4(b)), where the experimental data correspond to adsorption on samples of MCM-41 and SBA-15 with mean mesopore sizes of $D = 4.2$ nm and $D = 6.3$ nm (Thommes et al. 2007). We note that these pore diameters are substantially different from the one considered in our simulations ($D = 5.4$ nm) and thus we will be able to make only qualitative comparisons. Capillary condensation in model A occurs at relative pressures that are between those observed experimentally for samples with mesopore diameters below and above that of our model material. All our simulation models overestimate the amount adsorbed for Kr at $P/P_0 < 0.4$. For the case of Ar adsorption at 77 K, in Fig. 4(a) we compare our simulation results with experimental data (Galarneau et al. 2003) of adsorption on SBA-15 with a mean mesopore diameter of $D = 5$ nm (similar to that used in our models, $D = 5.4$ nm). Capillary condensation in model A takes place at relative pressures closer to those observed in experiments, and the amount adsorbed is overestimated in all our models at $P/P_0 < 0.7$. In the inset of Fig. 4(a), we compare the adsorption of Ar, in cm^3 of adsorbate (at standard T and P) per gram of adsorbent, between simulations and experiments. The amounts adsorbed in the experimental isotherm are close to those obtained from simulated Ar adsorption on pore model A; models B and C provide significantly lower adsorption at any given value of P/P_0. At 100% loading (high-pressure regime, $P/P_0 > 0.7$), there is excellent agreement between the experiment and the simulated adsorption isotherm on pore model A. In the experimental isotherm, capillary condensation takes place at values of P/P_0 between 0.55 and 0.74, which are comparable to those observed for the pore filling in model A ($P/P_0 \sim 0.60-0.67$). Nevertheless, the adsorption on pore model A at $P/P_0 < 0.7$ is larger than that reported in the experimental isotherm, as was the case for Kr at $P/P_0 < 0.4$. The lack of quantitative agreement between simulations and experiments for these pressure regimes could be due to at least two reasons. First, the intermolecular potential adsorbate-wall may be overestimating the attractive energy: for simulated Ar adsorption in regular cylindrical silica pores, it has been reported (Coasne and Pellenq 2004a, 2004b) that a reduction of 3% in selected parameters can lead to quantitative agreement in film thickness (t-plot) with experimental results. Second, the micropore volume and the degree of surface roughness for pore model A may be high when compared to the sample of SBA-15 used in the experimental measurements. We believe that tuning the micropore volume and/or the micropore size distribution in our model materials can lead to a better agreement with the experimental adsorption results.

Results for the isosteric heat of adsorption q_{st} are presented in Fig. 5 for Ar at 77 K and Kr at 87 K. These curves are typical of adsorption on heterogeneous surfaces, as they decrease down to a plateau value that is close to the heat of liquefaction of bulk Ar and Kr. In Fig. 5 we also show experimental data (Neimark et al. 1998) for Ar on MCM-41 with mesopores of about 4.5 nm, at 87 K. For Kr, the experimental value of q_{st} at low coverages is 15 kJ/mol (Pellenq and Levitz 2002). The experimental data for q_{st} for both Ar and Kr adsorption matches better our simulation results in pore model C. At low pore filling fractions ($N/N_0 < 0.3$), the total q_{st} in pore model A is larger than that observed for model B, which in turn is larger than that for model C (Fig. 5, left). The reason behind this observation is that the adsorbate-wall contribution to q_{st} for pore model A is significantly larger than that for model B; model C exhibits the lowest adsorbate-wall contribution to q_{st} (Fig. 5, right). As a result, the largest adsorption at a given pressure prior to capillary condensation is given by pore model A, followed by models B and C. Our results for q_{st}, as well as the comparison with experimental results, corroborate our prior conclusion that the micropore volume and the degree of surface roughness for pore model A is somewhat high, when compared to the two experimental samples of mesoporous silica used in the experimental measurements. It must be noted that the disagreement between the experimental results and those from models A and B, can also be explained by the large density of OH groups in the simulation models (7–8 OH/nm^2)

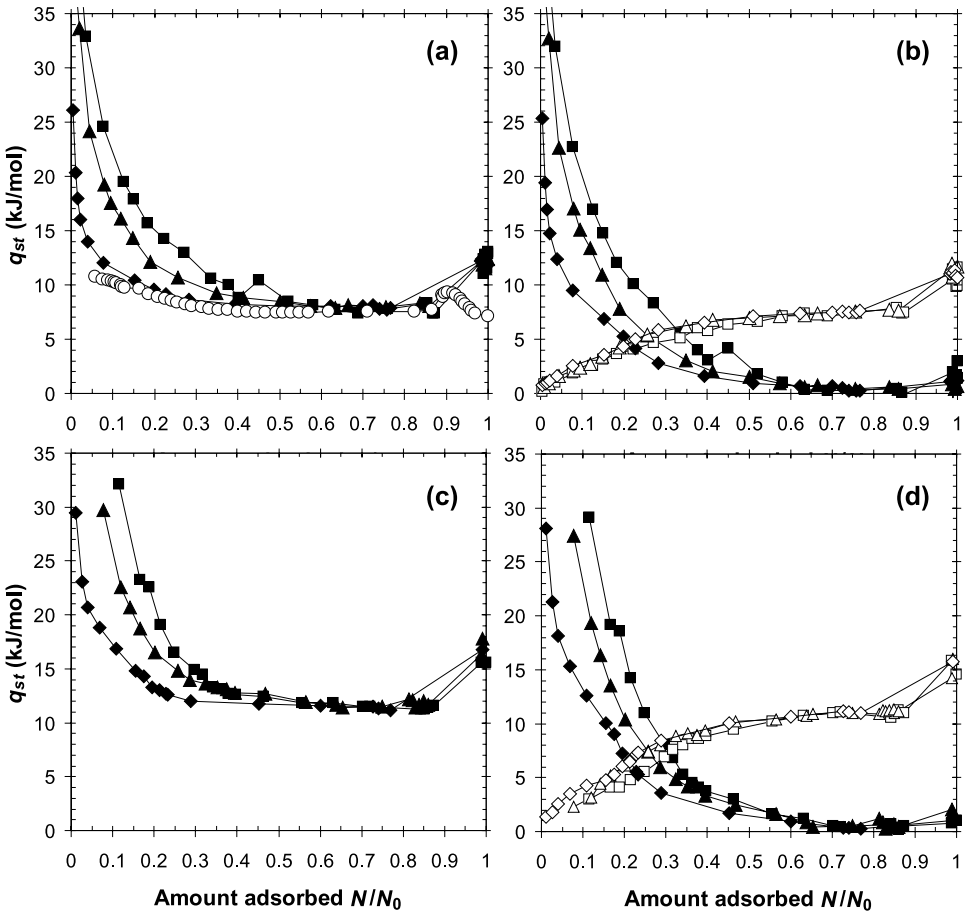

Fig. 5 Isosteric heat of adsorption q_{st} as a function of coverage fraction N/N_0, for Ar at 77 K (*top*), and Kr at 87 K (*bottom*). (**a**) and (**c**): total q_{st}; (**b**) and (**d**) adsorbate-wall (*black symbols*) and adsorbate-adsorbate (*white symbols*) contributions to q_{st}. *Squares*, *triangles* and *diamonds* represent simulation results for pore models A, B and C. Experimental results for Ar at 87 K on MCM-41 with mesopores of about 4.5 nm (Neimark et al. 1998) are depicted by *white circles* in Fig. 5(a)

that leads to a surface that is somewhat too attractive energetically. For instance, it has been shown that the adsorbed amount at a given pressure is reduced by a factor of 2 or 3 when the surface density of OH groups is decreased from 7 to 2 OH/nm^2 (Coasne et al. 2007). We also note that in our previous work (Coasne et al. 2006b) we obtained simulated SANS results for a similar silica mesopore model, and found that its roughness at length scales between 10 Å and 50 Å is in agreement with experimental measurements for templated mesoporous silica materials (Edler et al. 1998; Sonwane et al. 1999).

3.2 Discussion of the pore filling mechanisms

We have used our pore models to discuss the effect of surface roughness and structural defects on the pore filling mechanism. In Figs. 6 and 7 we present plots of representative simulation snapshots for Kr adsorption on pore models A and B, respectively, at $T = 87$ K and different values of P/P_0. The snapshots for Ar adsorption are qualitatively similar and thus are not included here. The pore filling mechanism on model C corresponds to the classical picture of capillary condensation in regular mesopores: the thickness of the adsorbed film increases with P/P_0 until it reaches its stability limit ($P/P_0 = 0.44$, Fig. 4(b)). A slight increase in P/P_0 makes the pore to be suddenly filled with a condensed phase and a vertical jump is observed in the adsorption isotherm ($P/P_0 = 0.46$, Fig. 4(b)).

For pore model A, at low relative pressures the Kr molecules are mainly adsorbed inside the micropores, whereas little adsorption takes place on the surface of the mesopores ($P/P_0 = 5 \times 10^{-7}$, Fig. 6(a)). As the pressure increases, the micropores fill and a monolayer of Kr covers the mesopore surface. The thickness of the Kr film adsorbed in the mesopores increases gradually with P/P_0, until it reaches the onset of capillary condensation in the mesopore at the center of the simulation box ($P/P_0 = 0.42$, Fig. 6(b)). A small increase in pressure causes capillary condensation in the central pore; however, the second pore still exhibits a low-density region in its center ($P/P_0 = 0.44$, Fig. 6(c)). A relative pressure of 0.52 is required to induce capillary condensation in the second pore ($P/P_0 = 0.52$, Fig. 6(d)). The adsorption mechanism on model B is very similar to what was described for the mesopores in model A: as P/P_0 increases, the pore walls are covered by an adsorbate film ($P/P_0 = 0.01$, Fig. 7(a)), whose thickness increases gradually with pressure ($P/P_0 = 0.32$, Fig. 7(b)). As was observed for model A, a small increase in P/P_0 induces capillary con-

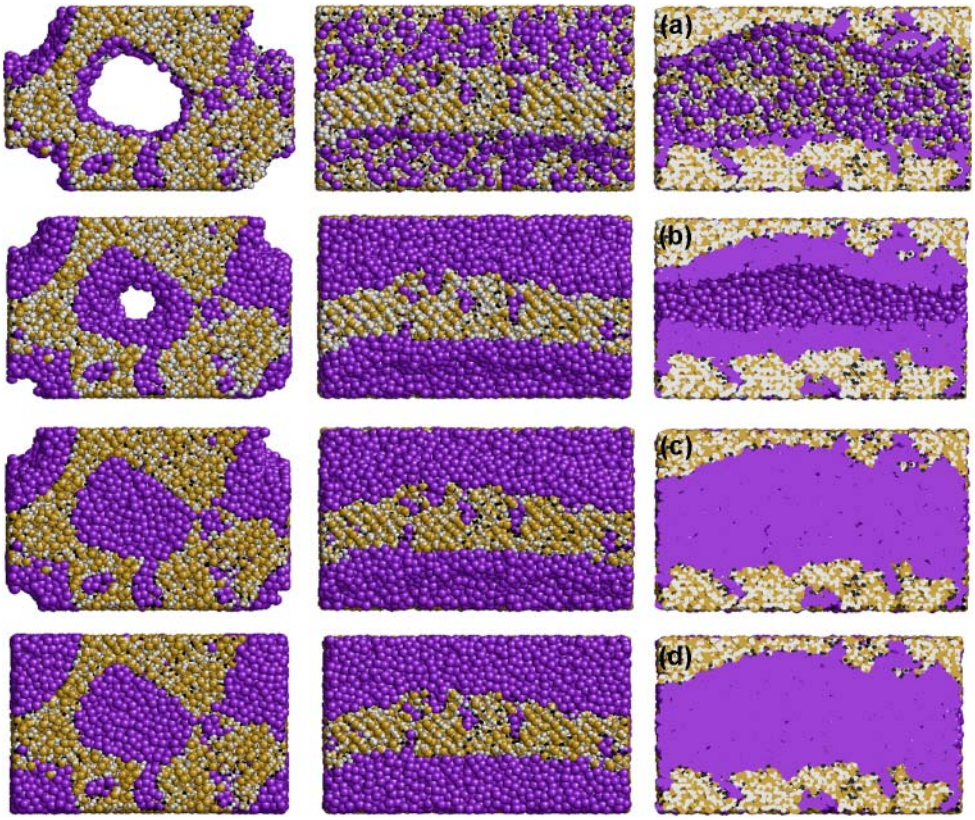

Fig. 6 (Color online) Representative simulation snapshots of Kr adsorbed on pore model A: front views (*left*), side views (*center*) and transverse section views of the center pore (*right*). Different values of relative pressure P/P_0 are depicted: (**a**) $P/P_0 = 5 \times 10^{-7}$, (**b**) $P/P_0 = 0.42$, (**c**) $P/P_0 = 0.44$, and (**d**) $P/P_0 = 0.52$. Silicon, oxygen, hydrogen and krypton atoms are depicted in *tan*, *white*, *black* and *purple*, respectively

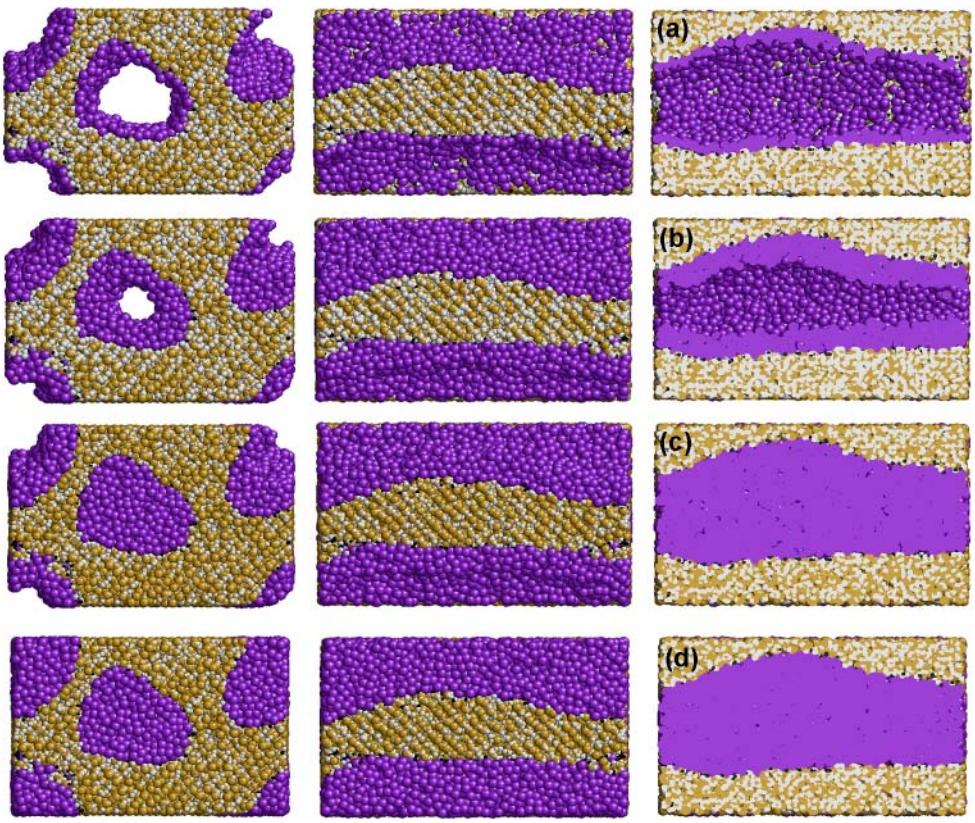

Fig. 7 (Color online) Representative simulation snapshots of Kr adsorbed on pore model B: front views (*left*), side views (*center*) and transverse section views of the center pore (*right*). Different values of relative pressure P/P_0 are depicted: (**a**) $P/P_0 = 0.01$, (**b**) $P/P_0 = 0.32$, (**c**) $P/P_0 = 0.36$, and (**d**) $P/P_0 = 0.48$. Silicon, oxygen, hydrogen and krypton atoms are depicted in *tan*, *white*, *black* and *purple*, respectively

densation in the central pore ($P/P_0 = 0.36$, Fig. 7(c)), and larger pressures are needed to fill the second pore with condensed Kr ($P/P_0 = 0.48$, Fig. 7(d)). Capillary condensation in the mesopores of model B take place at smaller values of relative pressure than in model A. Again, this is due to the fact that elimination of microporosity in model B leads to a small reduction in its mesopore diameters, as compared to those of model A (see the cross section views in Fig. 3). The two jumps observed in the adsorption isotherms for model A and B (Fig. 4) are therefore due to capillary condensation in the two pores (Fig. 3), which take place at different values of P/P_0 due to small differences in the pore morphologies. The adsorption isotherm is therefore expected to become smoother for a larger porous sample with a number of pores exhibiting small differences in their morphologies.

In our previous studies of gas adsorption on a single silica mesopore with significant surface roughness at length scales below 10 Å, (Coasne et al. 2005, 2006b; Hung et al. 2006), we observed phases that involved coexistence of liquid-like "bridges" and gas-like regions, just before capillary condensation took place, in analogy to what was found in past studies for adsorbents with distinct chemical and morphological heterogeneities (Bock and Schoen 1999; Sarkisov and Monson 2001; Pellenq and Levitz 2002; Detcheverry et al. 2003; Vishnyakov and Neimark 2003; Coasne and Pellenq 2004a, 2004b; Puibasset 2005b). In the present study, however, we did not observe any evidence of such intermediate phases. The filling of the mesopores in model materials A and B proceeded via a classical capillary condensation mechanism, where the pores fill at slightly different pressures. These results suggest that pore surface roughness, and other morphological features such as mesopore constrictions, play an important role in determining the mechanism of filling of the mesopores during gas adsorption.

4 Concluding remarks

In this work we report molecular simulation results for argon and krypton adsorption on atomistic models of templated mesoporous silica materials. These models add atomistic levels of detail to mesoscale representations of these porous materials, which were originally generated from lattice Monte Carlo simulations mimicking the synthesis process of templated mesoporous silicas (Bhattacharya and Gubbins 2005). We have generated our atomistic pore models by carving out of a silica block a 'mathematically-smooth' representation of the mesopores and micropores obtained from lattice MC simulations, as suggested in our previous studies (Coasne et al. 2005, 2006b; Hung et al. 2006). A model material with mean mesopore and micropore diameters of 5.4 nm and 1.1 nm was generated with that procedure (model A). Two additional model materials were considered: model B is the same as model A but with no microporosity, and model C consisted of a regular cylindrical mesopore with a diameter of 5.4 nm. We determined simulated isotherms and isosteric heats, for Ar and Kr adsorption on the three model materials at 77 K and 87 K, respectively, and compared with experimental data available for gas adsorption on SBA-15 and MCM-41 materials with similar mean mesopore diameters. The gas adsorption isotherms on model A were in good agreement with experimental data, while the isotherms obtained from models B and C seem to underestimate the adsorbed amounts (in cm^3 of adsorbate at standard T and P, per gram of adsorbent). For Ar adsorption, where the model materials and the experimental samples exhibited very similar mean mesopore diameters, we found excellent agreement in the adsorption at high pressures (100% loading) and in the capillary condensation pressure; however, the simulated adsorption at low and intermediate pressures were overestimated when compared with experiments. We argue that the micropore volume and the degree of surface roughness for pore model A may be somewhat high when compared to the samples of SBA-15 used in the experimental measurements. Results for the isosteric heat provide additional support for that conclusion. We believe that either fine-tuning the amount of microporosity or changing the surface chemistry (by decreasing the density of OH groups at the pore surface) in our model can lead to a better agreement with experiments, especially at low and intermediate pressures.

Our results also suggest that microporosity, surface roughness and structural defects (such as undulations in the mesopore surface, and pore constrictions) can affect significantly the gas adsorption. We observed marked differences in the adsorption isotherms, isosteric heat curves and pore filling mechanisms among the three model materials. For models A and B, which exhibit two mesopores each, we observed that small differences in their morphology lead to slightly different capillary condensation pressures. Moreover, elimination of microporosity in model B also induced a small reduction in its mesopore diameters. This caused capillary condensation to take place at pressures that are slightly lower than those observed for model A. The mesopore filling in these models proceeded via a classical capillary condensation mechanism, which contrasts to what was observed in our previous studies (Coasne et al. 2005, 2006b; Hung et al. 2006), where the pore filling of a silica mesopore with an important degree of surface roughness at length scales below 10 Å took place via a quasi-continuous pore filling involving coexistence of liquid-like "bridges" and gas-like regions. These results suggest that pore surface roughness, and other morphological features such as mesopore constrictions, play an important role in determining the mechanism of filling of the mesopores during gas adsorption. A detailed investigation of the structure of the dense phases inside these pores is currently in progress.

Acknowledgements This work was supported by a grant from the U.S. National Science Foundation (CTS-0626031). Supercomputing resources were made available from HPC-NCSU and the San Diego Supercomputing Center through NSF/MRAC grant CHE050047S.

References

Agrawal, R., Kofke, D.A.: Thermodynamic and structural properties of model systems at solid-fluid coexistence, II: melting and sublimation of the Lennard–Jones system. Mol. Phys. **85**, 43–59 (1995)

Allen, M.P., Tildesley, D.J.: Computer Simulation of Liquids. Clarendon, Oxford (1987)

Berenguer-Murcia, Á., García-Martínez, J., Cazorla-Amorós, D., Martínez-Alonso, A., Tascón, J.M.D., Linares-Solano, Á.: About the exclusive mesoporous character of MCM-41. Stud. Surf. Sci. Catal. **144**, 83–90 (2002)

Bhattacharya, S., Gubbins, K.E.: Modeling triblock surfactant-templated mesostructured cellular foams. J. Chem. Phys. **123**, 134907 (2005)

Bhattacharya, S., Gubbins, K.E.: Fast method for computing pore size distributions of model materials. Langmuir **22**, 7726–7731 (2006)

Bhattacharya, S., Coasne, B., Hung, F.R., Gubbins, K.E.: Molecular modeling of templated mesoporous materials, SBA-15, I: from mesoscopic to molecular models. Langmuir (2007, to be submitted)

Bock, H., Schoen, M.: Phase behavior of a simple fluid confined between chemically corrugated substrates. Phys. Rev. E **59**, 4122–4136 (1999)

Chiu, C.Y., Chiang, A.S.T., Chao, K.J.: Mesoporous silica powders and films—pore size characterization by krypton adsorption. Microporous Mesoporous Mater. **91**, 244–253 (2006)

Ciesla, U., Schüth, F.: Ordered mesoporous materials. Microporous Mesoporous Mater. **27**, 131–149 (1999)

Coasne, B., Pellenq, R.J.-M.: Grand canonical Monte Carlo simulation of argon adsorption at the surface of silica nanopores: effect of pore size, pore morphology, and surface roughness. J. Chem. Phys. **120**, 2913–2922 (2004a)

Coasne, B., Pellenq, R.J.-M.: A grand canonical Monte Carlo study of capillary condensation in mesoporous media: Effect of the pore morphology and topology. J. Chem. Phys. **121**, 3767–3774 (2004b)

Coasne, B., Gubbins, K.E., Pellenq, R.J.-M.: A grand canonical Monte Carlo study of adsorption and capillary phenomena in nanopores of various morphologies and topologies: testing the BET and BJH characterization methods. Part. Part. Syst. Charact. **21**, 149–160 (2004)

Coasne, B., Hung, F.R., Siperstein, F.R., Gubbins, K.E.: Molecular simulation of gas adsorption in realistic models of silica nanopores. Ann. Chim. Sci. Mater. **30**, 375–383 (2005)

Coasne, B., Hung, F.R., Pellenq, R.J.-M., Siperstein, F.R., Gubbins, K.E.: Adsorption of simple gases in MCM-41 materials: the role of surface roughness. Langmuir **22**, 194–202 (2006a)

Coasne, B., Galarneau, A., Di Renzo, F., Pellenq, R.J.-M.: Gas adsorption in mesoporous micelle-templated silicas: MCM-41, MCM-48, and SBA-15. Langmuir **22**, 11097–11105 (2006b)

Coasne, B., Galarneau, A., Di Renzo, F., Pellenq, R.J.-M.: Effect of surface chemistry on the adsorption of simple fluids on silica surfaces and nanopores. Langmuir (2007, to be submitted)

de Soler-Illia, G.J.A.A., Sanchez, C., Lebeau, B., Patarin, J.: Chemical strategies to design textured materials: from microporous and mesoporous oxides to nanonetworks and hierarchical structures. Chem. Rev. **102**, 4093–4138 (2002)

Detcheverry, F., Kierlik, E., Rosinberg, M.L., Tarjus, G.: Local mean-field study of capillary condensation in silica aerogels. Phys. Rev. E **68**, 061504 (2003)

Edler, K.J., Reynolds, P.A., White, J.W.: Small-angle neutron scattering studies on the mesoporous molecular sieve MCM-41. J. Phys. Chem. B **102**, 3676–3683 (1998)

Evans, R.: Fluids adsorbed in narrow pores—phase-equilibria and structure. J. Phys.: Condens. Matter **2**, 8989–9007 (1990)

Frenkel, D., Smit, B.: Understanding Molecular Simulation: from Algorithms to Applications, 2nd edn. Academic Press, London (2002)

Galarneau, A., Cambon, H., Di Renzo, F., Fajula, F.: True microporosity and surface area of mesoporous SBA-15 silicas as a function of synthesis temperature. Langmuir **17**, 8328–8335 (2001)

Galarneau, A., Cambon, H., Renzo, F.D., Ryoo, R., Choi, M., Fajula, F.: Microporosity and connections between pores in SBA-15 mesostructured silicas as a function of the temperature of synthesis. New J. Chem. **27**, 73–79 (2003)

Gelb, L.D.: The ins and outs of capillary condensation in cylindrical pores. Mol. Phys. **100**, 2049–2057 (2002)

Gelb, L.D., Gubbins, K.E.: Characterization of porous glasses: simulation models, adsorption isotherms, and the Brunauer–Emmett–Teller analysis method. Langmuir **14**, 2097–2111 (1998)

Gelb, L.D., Gubbins, K.E.: Correlation functions of adsorbed fluids in porous glass: a computer simulation study. Mol. Phys. **96**, 1795–1804 (1999a)

Gelb, L.D., Gubbins, K.E.: Pore size distributions in porous glasses: a computer simulation study. Langmuir **15**, 305–308 (1999b)

Gelb, L.D., Gubbins, K.E., Radhakrishnan, R., Sliwinska-Bartkowiak, M.: Phase separation in confined systems. Rep. Prog. Phys. **62**, 1573–1659 (1999)

Gregg, S.J., Sing, K.S.W.: Adsorption, Surface Area and Porosity, 2nd edn. Academic Press, London (1982)

He, Y., Seaton, N.A.: Experimental and computer simulation studies of the adsorption of ethane, carbon dioxide, and their binary mixtures in MCM-41. Langmuir **19**, 10132–10138 (2003)

Hung, F.R., Coasne, B., Gubbins, K.E., Siperstein, F.R., Thommes, M., Sliwinska-Bartkowiak, M.: A Monte Carlo study of capillary condensation of krypton within realistic models of templated mesoporous silica materials. Stud. Surf. Sci. Catal. **160**, 153–161 (2006)

Imperor-Clerc, M., Davidson, P., Davidson, D.A.: Existence of a microporous corona around the mesopores of silica-based SBA-15 materials templated by triblock copolymers. J. Am. Chem. Soc. **122**, 11925–11933 (2000)

Johnson, J.K., Zollweg, J.A., Gubbins, K.E.: The Lennard–Jones equation of state revisited. Mol. Phys. **78**, 591–618 (1993)

Jun, S., Joo, S.H., Ryoo, R., Kruk, M., Jaroniec, M., Liu, Z., Ohsuna, T., Terasaki, O.: Synthesis of new, nanoporous carbon with hexagonally ordered mesostructure. J. Am. Chem. Soc. **122**, 10712–10713 (2000)

Kofke, D.A.: Direct evaluation of phase coexistence by molecular simulation via integration along the saturation line. J. Chem. Phys. **98**, 4149–4162 (1993)

Koh, C.A., Montanari, T., Nooney, R.I., Tahir, S.F., Westacott, R.E.: Experimental and computer simulation studies of the removal of carbon dioxide from mixtures with methane using AlPO4-5 and MCM-41. Langmuir **15**, 6043–6049 (1999)

Kresge, C.T., Leonowicz, M.E., Roth, W.J., Vartuli, J.C., Beck, J.S.: Ordered mesoporous molecular sieves synthesized by a liquid-crystal template mechanism. Nature **359**, 710–712 (1992)

Kruk, M., Jaroniec, M., Sayari, A.: Application of large pore MCM-41 molecular sieves to improve pore size analysis using nitrogen adsorption measurements. Langmuir **13**, 6267–6273 (1997)

Kuchta, B., Llewellyn, P., Denoyel, R., Firlej, L.: Modeling of pore wall amorphous structures: influence of wall heterogeneity on the mechanism of adsorption—krypton and argon adsorption in MCM-41 pore model. Colloid Surf. A **241**, 137–142 (2004)

Landmesser, H., Kosslick, H., Storek, W., Frick, R.: Interior surface hydroxyl groups in ordered mesoporous silicates. Solid State Ionics **101–103**, 271–277 (1997)

Llewellyn, P.L., Grillet, Y., Rouquerol, J., Martin, C., Coulomb, J.-P.: Thermodynamic and structural properties of physisorbed phases within the model mesoporous adsorbent M4IS (pore diameter 2.5 nm). Surf. Sci. **352–354**, 468–474 (1996)

Llewellyn, P.L., Sauerland, C., Martin, C., Grillet, Y., Coulomb, J.-P., Rouquerol, F., Rouquerol, J.: A thermodynamic investigation of physisorbed phases within the model mesoporous material: MCM-41. In: McEnaney, B., Mays, T.J., Rouquerol, J., Rodríguez-Reinoso, F., Sing, K.S.W., Unger, K.K. (eds.) Characterisation of Porous Solids IV, pp. 111–117. The Royal Society of Chemistry, Cambridge (1997)

Lísal, M., Hall, C.K., Gubbins, K.E., Panagiotopoulos, A.Z.: Self-assembly of surfactants in a supercritical solvent from lattice Monte Carlo simulations. J. Chem. Phys. **116**, 1171–1184 (2002)

Maddox, M.W., Olivier, J.P., Gubbins, K.E.: Characterization of MCM-41 using molecular simulation: heterogeneity effects. Langmuir **13**, 1737–1745 (1997)

Neimark, A.V., Ravikovitch, P.I., Grün, M., Schüth, F., Unger, K.K.: Pore size analysis of MCM-41 type adsorbents by means of nitrogen and argon adsorption. J. Colloid Interface Sci. **207**, 159–169 (1998)

Nicholson, D., Parsonage, N.G.: Computer Simulation and the Statistical Mechanics of Adsorption. Academic Press, London (1982)

Pellenq, R.J.-M., Levitz, P.E.: Capillary condensation in a disordered mesoporous medium: a grand canonical Monte Carlo study. Mol. Phys. **100**, 2059–2077 (2002)

Pellenq, R.J.-M., Nicholson, D.: Intermolecular potential function for the physical adsorption of rare gases in silicalite. J. Phys. Chem. **98**, 13339–13349 (1994)

Piegl, L.A., Tiller, W.: The NURBS Book, 2nd edn. Springer, Berlin (1997)

Puibasset, J.: Grand potential, Helmholtz free energy, and entropy calculation in heterogeneous cylindrical pores by the grand canonical Monte Carlo simulation method. J. Phys. Chem. B **109**, 480–487 (2005a)

Puibasset, J.: Phase coexistence in heterogeneous porous media: a new extension to Gibbs ensemble Monte Carlo simulation method. J. Chem. Phys. **122**, 134710 (2005b)

Rouquerol, F., Rouquerol, J., Sing, K.: Adsorption by powders and porous solids. Academic Press, London (1999)

Ryoo, R., Ko, C.H., Kruk, M., Antochshuk, V., Jaroniec, M.: Block-copolymer-templated ordered mesoporous silica: array of uniform mesopores or mesopore-micropore network? J. Phys. Chem. B **104**, 11465–11471 (2000)

Sarkisov, L., Monson, P.A.: Modeling of adsorption and desorption in pores of simple geometry using molecular dynamics. Langmuir **17**, 7600–7604 (2001)

Scanu, L.F., Gubbins, K.E., Hall, C.K.: Lattice Monte Carlo simulations of phase separations and micellization in supercritical CO_2/surfactant systems: effect of CO_2 density. Langmuir **20**, 514–523 (2004)

Schumacher, C., Gonzalez, J., Wright, P.A., Seaton, N.A.: Generation of atomistic models of periodic mesoporous silica by kinetic Monte Carlo simulation of the synthesis of the material. J. Phys. Chem. B **110**, 319–333 (2006a)

Schumacher, C., Gonzalez, J., Pérez-Mendoza, M., Wright, P.A., Seaton, N.A.: Design of hybrid organic/inorganic adsorbents based on periodic mesoporous silica. Ind. Eng. Chem. Res. **45**, 5586–5597 (2006b)

Schüth, F., Schmidt, W.: Microporous and mesoporous materials. Adv. Mater. **14**, 629–638 (2002)

Selvam, P., Bhatia, S.K., Sonwane, C.G.: Recent advances in processing and characterization of periodic mesoporous MCM-41 silicate molecular sieves. Ind. Eng. Chem. Res. **40**, 3237–3261 (2001)

Siperstein, F.R., Gubbins, K.E.: Synthesis and characterization of templated mesoporous materials using molecular simulation. Mol. Simul. **27**, 339–352 (2001)

Siperstein, F.R., Gubbins, K.E.: Phase separation and liquid crystal self-assembly in surfactant-inorganic-solvent systems. Langmuir **19**, 2049–2057 (2003)

Sonwane, C.G., Bhatia, S.K., Calos, N.J.: Characterization of surface roughness of MCM-41 using methods of fractal analysis. Langmuir **15**, 4603–4612 (1999)

Sonwane, C.G., Jones, C.W., Ludovice, P.J.: A model for the structure of MCM-41 incorporating surface roughness. J. Phys. Chem. B **109**, 23395–23404 (2005)

Takei, T., Chikazawa, M.: Measurement of pore size distribution of low-surface-area materials by krypton gas adsorption method. J. Ceram. Soc. Jpn. **106**, 353–357 (1998)

Thommes, M.: Physical adsorption characterization of ordered and amorphous mesoporous materials. In: Lu, G.Q., Zhao, X.S. (eds.) Nanoporous Materials: Science and Engineering, pp. 317–364. Imperial College Press, London (2004)

Thommes, M., Nishiyama, N., Tanaka, S.: Aspects of a novel method for the pore size analysis of thin silica films based on krypton adsorption at liquid argon temperature (87.3 K). Stud. Surf. Sci. Catal. (2007, in press)

Vishnyakov, A., Neimark, A.V.: Monte Carlo simulation test of pore blocking effects. Langmuir **19**, 3240–3247 (2003)

Zhao, D., Feng, J., Huo, Q., Melosh, N., Fredrickson, G.H., Chmelka, B.F., Stucky, G.D.: Triblock copolymer syntheses of mesoporous silica with periodic 50 to 300 Angstrom pores. Science **279**, 548–552 (1998a)

Zhao, D., Huo, Q., Feng, J., Chmelka, B.F., Stucky, G.D.: Nonionic triblock and star diblock copolymer and oligomeric surfactant syntheses of highly ordered, hydrothermally stable, mesoporous silica structures. J. Am. Chem. Soc. **120**, 6024–6036 (1998b)

Zukal, A.: Adsorption and pore condensation of krypton on mesoporous silicas at 77 K. Microporous Mesoporous Mater. **92**, 220–226 (2006)